Combustion and Flame xxx (2010) xxx–xxx

Contents lists available at ScienceDirect

Combustion and Flame

journal homepage: www.elsevier.com/locate/combustflame

Extinction of premixed methane/air flames in microgravity by diluents: Effects of radiation and Lewis number

L. Qiao [a,*], Y. Gan [a], T. Nishiie [a], W.J.A. Dahm [b], E.S. Oran [c]

[a] School of Aeronautics & Astronautics, Purdue University, West Lafayette, IN 47907-2045, USA
[b] Department of Aerospace Engineering, The University of Michigan, Ann Arbor, MI 48109-2140, USA
[c] Laboratory for Computational Physics and Fluid Dynamics, Naval Research Laboratory, Washington, DC 20375, USA

ARTICLE INFO

Article history:
Received 13 May 2009
Received in revised form 24 June 2009
Accepted 6 April 2010
Available online xxxx

Keywords:
Extinction
Microgravity
Inert gases
Lewis number
Radiation and reabsorption
Chemical suppression

ABSTRACT

Laminar burning velocities and flammability limits of premixed methane/air flames in the presence of various diluents were investigated by combined use of experiments and numerical simulations. The experiments used a 1-m free-fall spherical combustion chamber to eliminate the effect of buoyancy, enabling accurate measurements of near-limit burning velocities and flammability limits. Burning velocities were measured for CH_4/air flames with varying concentrations of He, Ar, N_2 and CO_2 at NTP. The limiting concentration of each diluent was measured by systematically varying the composition and ignition energy and finding the limiting condition through successive experiment trials. The corresponding freely-propagating, planar 1-D flames were simulated using PREMIX. The transient spherically-expanding flames were simulated using the 1-D Spherical Flame & Reactor Module of COSILAB considering detailed radiation models. The results show that helium exhibits more complex limit behavior than the other diluents due to the large Lewis number of helium mixtures. The near-limit helium-diluted flames require much higher ignition energy than the other flames. In addition, for the spherically expanding helium-diluted flames studied here ($Le > 1$), stretch suppresses flame propagation and may cause flame extinction. For the CO_2-diluted flames, the flame speed predicted by the optically-thick model based on the Discrete Transfer Method (DTW) and a modified wide band model has better agreement with measurements in the near-limit region. A significant amount of heat is absorbed by the dilution gas CO_2, resulting in elevation of temperature of the ambient gases. The optically-thick model, however, still overpredicts flame speed, indicating a more sophisticated radiation property model may be needed. Finally, the chemical effect of CO_2 on flame suppression was quantified by a numerical analysis. The results show that the chemical effect of CO_2 is more important than the other diluents due to its active participation in the reaction $CO_2 + H = CO + OH$, which competes for H radicals with the chain-branching reactions and thus reduces flame speed.

1. Introduction

The inert gases such as helium, argon, nitrogen, and carbon dioxide are an important class of fire extinguishing agents because they are natural, non-ozone-depleting, non-toxic and non-pyrolytic gases. Such gases may be essential, for example, for extinguishing fires in confined environments such as spacecraft. The extinguishing mechanisms of these diluents have been studied experimentally and computationally for various flame configurations at terrestrial or microgravity conditions [1–8].

Laminar burning velocity and flammability limits of premixed flames are key parameters of both fundamental and practical significance. Accurate measurement of unstretched laminar burning velocity is necessary for assessing combustion theories and the validation of numerical models. Numerous studies have shown that gravity has significant influence on near-limit behavior of laminar and turbulent flames [9–13]. Ronney [13] provided a comprehensive review on premixed-gas flames in microgravity. Generally, the flammability limits obtained at 1-g and μ-g are different. Burning velocities of near-limit flames are difficult to measure at 1-g because the natural convection causes severe flame-front distortion. For example, the outwardly-propagating spherical flames, which have been traditionally used to measure flame speed, would propagate upward at limit conditions and form a mushroom shape due to buoyant convection.

In a previous study [14] we presented results from a 1-m free-fall experiment that eliminated the effect of buoyancy on premixed flames. Those experiments used a stationary shadowgraph system to image flame propagation inside a dropping spherical chamber.

* Corresponding author. Address: School of Aeronautics & Astronautics, Purdue University, 701W. Stadium Ave., West Lafayette, IN 47907-2045, USA. Fax: +1 765 494 0307.
E-mail address: lqiao@ecn.purdue.edu (L. Qiao).

0010-2180/$ - see front matter © 2010 The Combustion Institute. Published by Elsevier Inc. All rights reserved.
doi:10.1016/j.combustflame.2010.04.004

Report Documentation Page

Form Approved
OMB No. 0704-0188

1. REPORT DATE	2. REPORT TYPE	3. DATES COVERED
2010		**00-00-2010 to 00-00-2010**

4. TITLE AND SUBTITLE	5a. CONTRACT NUMBER
Extinction of premixed methane/air flames in microgravity by diluents: Effects of radiation and Lewis number	5b. GRANT NUMBER
	5c. PROGRAM ELEMENT NUMBER
6. AUTHOR(S)	5d. PROJECT NUMBER
	5e. TASK NUMBER
	5f. WORK UNIT NUMBER
7. PERFORMING ORGANIZATION NAME(S) AND ADDRESS(ES) **School of Aeronautics & Astronautics,Purdue University,West Lafayette,IN,47907-2045**	8. PERFORMING ORGANIZATION REPORT NUMBER
9. SPONSORING/MONITORING AGENCY NAME(S) AND ADDRESS(ES)	10. SPONSOR/MONITOR'S ACRONYM(S)
	11. SPONSOR/MONITOR'S REPORT NUMBER(S)

12. DISTRIBUTION/AVAILABILITY STATEMENT
Approved for public release; distribution unlimited

13. SUPPLEMENTARY NOTES

14. ABSTRACT

Laminar burning velocities and flammability limits of premixed methane/air flames in the presence of various diluents were investigated by combined use of experiments and numerical simulations. The experiments used a 1-m free-fall spherical combustion chamber to eliminate the effect of buoyancy, enabling accurate measurements of near-limit burning velocities and flammability limits. Burning velocities were measured for CH4/air flames with varying concentrations of He, Ar, N2 and CO2 at NTP. The limiting concentration of each diluent was measured by systematically varying the composition and ignition energy and finding the limiting condition through successive experiment trials. The corresponding freelypropagating, planar 1-D flames were simulated using PREMIX. The transient spherically-expanding flames were simulated using the 1-D Spherical Flame & Reactor Module of COSILAB considering detailed radiation models. The results show that helium exhibits more complex limit behavior than the other diluents due to the large Lewis number of helium mixtures. The near-limit helium-diluted flames require much higher ignition energy than the other flames. In addition, for the spherically expanding heliumdiluted flames studied here (Le > 1), stretch suppresses flame propagation and may cause flame extinction. For the CO2-diluted flames, the flame speed predicted by the optically-thick model based on the Discrete Transfer Method (DTW) and a modified wide band model has better agreement with measurements in the near-limit region. A significant amount of heat is absorbed by the dilution gas CO2, resulting in elevation of temperature of the ambient gases. The optically-thick model, however, still overpredicts flame speed, indicating a more sophisticated radiation property model may be needed. Finally, the chemical effect of CO2 on flame suppression was quantified by a numerical analysis. The results show that the chemical effect of CO2 is more important than the other diluents due to its active participation in the reaction CO2 + H = CO + OH, which competes for H radicals with the chain-branching reactions and thus reduces flame speed.

15. SUBJECT TERMS

16. SECURITY CLASSIFICATION OF:			17. LIMITATION OF ABSTRACT	18. NUMBER OF PAGES	19a. NAME OF RESPONSIBLE PERSON
a. REPORT **unclassified**	b. ABSTRACT **unclassified**	c. THIS PAGE **unclassified**	**Same as Report (SAR)**	**10**	

Standard Form 298 (Rev. 8-98)
Prescribed by ANSI Std Z39-18

Nomenclature

D	mass diffusivity	σ	Stefan–Boltzmann constant
K	flame stretch	k_p	Planck mean absorption coefficient
L	Markstein length	v	spectrum wave number
Ma	Markstein number, L/δ_D	M	total number of bands
δ_D	characteristic flame thickness, $D_u/S_{L\infty}$	N	total number of rays
r_f	flame radius	n	grid cell
t	time	kv	spectral absorption coefficient
S_L	local laminar burning velocity	κv	optical depth
$S_{L\infty}$	planar unstretched laminar burning velocity	I_{bv}	spectral blackbody radiation intensity
P	pressure	η	the spectrum
T	temperature	q_r	radiation heat source
T_0	ambient temperature	I	spectral blackbody radiation intensity
X	mole fraction	Ω	solid angle
ρ	density	$I_{n,i,j}$	radiation intensity of band j and ray i at grid n
ϕ	fuel-equivalence ratio		

The near-limit flames maintained a spherical shape that allowed their laminar burning velocity to be inferred from the measured flame radius versus time. Measurements of near-limit burning velocities under microgravity conditions for H_2/air/diluent premixed flames at various fuel-equivalence ratios and pressures [15] were reported using this facility. The measured velocities were compared to calculations, which, when analyzed, revealed that inaccuracies in the three-body termination rates for $H + O_2 + M = HO_2 + M$ reactions and in mass diffusion coefficients for H_2 diffusion are the most likely explanation for the near-limit differences. In these studies [14,15], numerical simulations were performed for 1-D planar freely-propagating flames using PREMIX [16]. Radiative heat loss was either not considered or was simulated using a simple optically-thin model. The results show that radiative heat loss was insignificant for He, Ar, or N_2-diluted hydrogen/air flames. It, however, could be significant for CO_2-diluted flames. The reabsorption effect of CO_2 can affect near-limit behavior when CO_2 concentration is high. Furthermore, the 1-D planar flame simulation using PREMIX may not represent the spherical flames as investigated in the experiments, which are subject to flame stretch. Stretch, combined with radiation/reabsorption, could change flame dynamics and extinguishing processes. Therefore, a more sophisticated modeling that combines all these effects is desirable for a better interpretation of flame extinction behavior by diluents.

The combined effects of stretch and radiation on premixed flames have been studied by several researchers [17–35]. Farmer and Ronney [17] numerically examined the dynamics properties of near-limit CH_4/air flames in planar and spherical geometries considering radiative heat loss from CO_2 and H_2O. Their results show that spherical geometry simulations had good qualitative and quantitative agreement with results obtained in microgravity experiments. The results also show that the extinguishment processes at microgravity are a result of the interactions among the Lewis number effect, flame front curvature and heat loss due to gas radiation. Buckmaster [22] examined the behavior of twin premixed opposed-flow flames considering radiation heat loss. The numerical simulations captured a number of different flame responses for a wider range of mixture strength. Bechtold et al. [32] developed a general theory of non-adiabatic premixed flames of arbitrary shape that fully accounts for the hydrodynamic and diffusive-thermal processes and incorporates the effects of volumetric heat losses. Wang and Niioka [31] numerically investigated radiation reabsorption effects in CH_4–air counterflow premixed flames and found that the reabsorption of emitting radiation leads to substantially wider flame thickness and higher flame temperature than those calculated by using the optically-thin model. Ju and his co-workers [23–30,34,35] conducted extensive studies on the combined effects of radiation and stretch on flammability limits for various Lewis number mixtures. In particular, their recent work [34] show that the flame geometry has a significant impact on radiation absorption and that the 1-D planar radiation model was not valid for the computation of the flame speed of a spherical flame.

To validate radiation models and to understand the dynamics and extinction process of premixed flames, experimental data such as flame speed are useful, which, however, are not easy to obtain for near-limit flames because of buoyancy. In the present paper, measurements of laminar burning velocities and extinction limits for methane/air/diluent flames using the same 1-m free-fall facility were reported. The transient outwardly-propagating spherical flames were simulated using the Spherical Flame Module of COSILAB [36] with detailed radiation models. The objective was to understand how and when the premixed methane–air flames are extinguished by various inert gases (He, Ar, N_2 and CO_2), and in particular, to understand the effects of Lewis number, flame stretch, and radiation emission and absorption of CO_2 on flame propagation and extinction. Here measurements of burning velocities of stoichiometric methane/air/diluent mixtures at NTP at varying diluent concentrations are first presented. The measured velocities are then compared with numerical simulations. After that the measured concentration of each inert gas at the point at which the flame is extinguished is reported and is compared with the data in the literature. This limiting concentration was determined by systematically varying the composition and ignition energy and finding the limiting condition through successive experiment trials. The results show that helium behaves in a complex way at the limit due to its high diffusivities. Then the effects of radiation emission and absorption on the CO_2-diluted flames are discussed. The results show that the flame speed predicted based on the Discrete Transfer Method (DTM) and a modified wideband model is higher than that predicted by the optically-thin limit model. A significant amount of radiation heat loss from the hot products is reabsorbed by the cold ambient gases, resulting in temperature increase in the unburned gas and the pre-heat zone, which consequently increases reaction rate and flame speed. Finally, the pure chemical effect of CO_2 in flame suppression was quantified by a numerical analysis. The results show that the chemical effect of CO_2 can cause as much as 30% reduction in flame speed near extinction limits. This is because the competition of CO_2 for H radical through the reaction $CO + OH = CO_2 + H$ with the chain-branching reaction $H + O_2 = O + OH$ reduces H, OH, and O radical concentrations, leading to lower reaction rate and flame speed.

Please cite this article in press as: L. Qiao et al., Combust. Flame (2010), doi:10.1016/j.combustflame.2010.04.004

2. Experimental method

The experimental methods are similar to earlier work [14,15] and will be described only briefly here. The free-fall facility consists of a support tower, a free-falling spherical combustion chamber, a spark generator, a deceleration box, and shadowgraph optics that record the flame propagation as the chamber falls. The idea was to use a stationary optical system to image flame propagation inside a dropping chamber. The free-fall chamber was held at the top of the tower by an electromagnet before being dropped. As the chamber was released, a hall-effect sensor detected the motion and sent a trigger pulse to the delay generator. A short delay was then provided to allow oscillations from the chamber release to decay to sufficiently low levels. After the delay, the generator sent out two signals, one of which triggered a high-voltage spark generator connected to electrodes that ignited the mixture, and the other triggered a high-speed digital video camera which recorded shadowgraph images of the flame propagation within the free-falling chamber. The spark gap and spark energy were adjusted to be as close as possible to the minimum ignition energies.

The present measurements were restricted to flames having diameters 10 mm < d < 60 mm. The lower limit provides sufficient time for disturbances introduced by ignition to decay, while the upper limit limits the pressure rise in the chamber during the measuring period to less than 0.7% of the initial pressure. No results were considered where the flame surface appeared wrinkled due to flame instabilities. As in previous experiments, the measurements presented here were limited to $\delta_D/r_f < 0.05$ where δ_D is the characteristic flame thickness and r_f is flame radius. This minimizes effects of curvature and transient phenomena associated with large flame thickness during the early stages of flame formation. Under these assumptions, quasi-steady expressions for the local laminar burning velocity and flame stretch are given by [37]

$$S_L = \frac{\rho_b}{\rho_u}\frac{dr_f}{dt}, \quad K = \frac{2}{r_f}\frac{dr_f}{dt}, \tag{1}$$

where S_L is the observed stretched flame propagation speed into the unburned gas and K is the flame stretch. The density ratio needed to determine S_L was computed assuming adiabatic constant-pressure combustion with the same concentrations of elements in the unburned gases. These calculations were carried out using the adiabatic equilibrium algorithms of McBride et al. [38]. The flame propagation velocity, dr_f/dt, was obtained from the flame radius $r_f(t)$ as measured from the shadowgraph images along the direction perpendicular to the spark electrodes, where disturbances of the flame surface by the electrodes were minimal. From Markstein [39] and Clavin [40], the laminar burning velocity S_L is related to the flame stretch K for small to moderate values of curvature and stretch,

$$S_L = S_{L\infty} - LK. \tag{2}$$

The Markstein length L is a measure of the flame response to the stretch rate K, and it can be either positive (stable to preferential-diffusion) or negative (unstable to preferential-diffusion), depending on the reactants. The unstretched laminar burning velocities $S_{L\infty}$ were obtained by extrapolating the measured stretched laminar burning velocities $S_L(K)$ as a function of the local stretch rate K to zero stretch. The Markstein number Ma was obtained by normalizing L with a characteristic flame thickness δ_D defined as $D_u/S_{L\infty}$, where D_u is the mass diffusivity of fuel-oxidizer. For simplicity and consistency, we used the binary diffusivity of CH_4–O_2 (21.9 mm^2/s) for all mixtures including the helium-diluted flames, even though helium addition can change the mass diffusivity of the mixture significantly.

Experimental conditions for CH_4/air/diluent flames are summarized in Table 1, which shows reactant mixtures at room temperature (293 ± 0.5 K), a fuel-equivalence ratio of 1.0, a pressure of 1.0 atm, and diluent concentrations from 0% to the extinction limit for He, Ar, N_2 and CO_2.

3. Computational method

Numerical simulations of the corresponding planar unstretched premixed flames were carried out using the steady, 1-D laminar premixed flame code PREMIX [16]. CHEMKIN is used as a preprocessor to determine thermochemical and transport properties from the database of Kee et al. [41,42]. The simulations used the detailed chemical reaction mechanism GRI-Mech 3.0 [43], which involves 325 reactions and 53 species. Multi-component diffusion and variable thermodynamic properties were considered. The resulting computed unstretched burning velocities were compared for each diluent type and concentration with the corresponding measured values obtained as described above.

To evaluate the combined effects of chemical kinetics, radiation, and stretch on methane/air/diluent flames, we also simulated the outwardly-propagating spherical flames using the 1-D Spherical Flames Module of COSILAB, whose original version was called RUN1DL and was developed by Rogg and coworkers at Cambridge University [44]. The simulations are for reactant mixtures initially at room temperature 293 K and are for flame propagation at constant pressures. Similar to the 1-D planar flame simulations, GRI-Mech 3.0 was used in the transient simulations. CHEMKIN was used as a preprocessor to determine thermochemical and transport properties from the database of Kee et al. [16,41,42,45]. For the effective solution of time-dependent reactive-flow problems an extrapolation method called EULER [36] was used, which is based on algorithms suitable for the solution of differential algebraic systems. An adaptive gridding method was also used to improve computational efficiency.

The computational domain was set to have a radius of 8 cm. The reactant mixture was numerically ignited by a hot spot located at the origin. The size of the hot spot is typically below 1/10 of the computational domain, with larger spots used for near-extinction flames. After the reactant mixture was ignited, a propagating flame

Table 1
CH_4/air/diluent laminar premixed flame test conditions.[a]

Diluent	X_D	ρ_u/ρ_b	$S_{L\infty}$ (cm/s)	Le[b]
–	0.00	7.51	37.0	0.99
He	0.10	7.26	32.0	1.70
He	0.20	6.92	25.9	2.40
He	0.30	6.55	20.7	3.11
He	0.35	6.32	17.1	3.46
Ar	0.10	7.26	28.3	0.99
Ar	0.20	6.92	20.3	0.98
Ar	0.30	6.55	14.3	0.98
Ar	0.40	6.07	9.0	0.97
Ar	0.45	5.79	6.1	0.97
Ar	0.48	5.60	4.3	0.97
N_2	0.10	7.11	25.5	0.99
N_2	0.15	6.86	20.7	0.98
N_2	0.20	6.60	15.9	0.98
N_2	0.25	6.33	11.8	0.98
N_2	0.30	6.07	8.6	0.98
N_2	0.35	5.78	5.4	0.98
CO_2	0.05	7.15	19.2	0.97
CO_2	0.10	6.82	11.4	0.94
CO_2	0.15	6.46	9.0	0.92
CO_2	0.20	6.10	5.5	0.89
CO_2	0.22	5.96	4.4	0.89

[a] At P = 1.0 atm, ϕ = 1.0, and 298 ± 0.5 K.
[b] Lewis number is evaluated based on the thermal diffusivity of the reactant mixture and the binary mass diffusivity of CH_4–O_2 (21.9 mm^2/s).

was established, ahead of which was the quiescent unburned mixture and behind which were the combustion products. The hot spot temperature profile can be adjusted so that the amount of energy supplied to the reactant mixture can be varied to be close to the minimum ignition energy, similar to the experiment. For boundary conditions, the mole fraction of each gas has zero-gradient at the origin and has fixed values at the right boundary. To determine flame propagation speed, we chose the location where the temperature is 400 K to be flame front. The propagation speed of expanding flame surfaces, however, does not depend on the specific choice of flame position for thin flames according to a previous study [36]. The methodology to obtain unstretched laminar burning velocity and Markstein length from the outwardly-propagating spherical flame simulations were similar to the experiments, following Eqs. (1) and (2). To remove local disturbances introduced by the numerical scheme, the flame speed data were smoothed using LOWESS scheme [46] with a window size of 0.5. To avoid ignition disturbances, flame speed data were processed for $r > 1.5$ cm.

Radiation becomes increasingly important when flammability limits are approached. Therefore it needs special consideration in the present study which concerns flame extinction. A radiation model typically consists of a radiation property model for the radiative properties of gases and a radiative transfer model which solves the radiative transfer equation (RTE). Here, we employed two radiation models in the transient simulations using COSILAB: an optically-thin limit model and an optically-thick model based on the Discrete Transfer Method (DTM) [47], both in 1-D spherical coordinates. The optically-thin limit model basically assumes that radiation can pass through the medium without significant absorption. With gray gas assumption, for which a mean absorption coefficient is used over the entire wavelength spectrum, the optically-thin limit model can be simplified as [47]

$$\nabla \cdot q_r = k_p(T)(4\sigma T^4 - 4\sigma T_\infty^4) \tag{3}$$

where $\nabla \cdot q_r$ is the radiative heat loss rate per unit volume, k_P is the Planck mean absorption coefficient, σ is the Stefan–Boltzmann constant. Radiation of the gaseous species CO_2, H_2O, and CO were considered and their absorption coefficients were taken from [48].

The details of the Discrete Transfer Method (DTM) are discussed in Ref. [47] and will be briefly described here. The DTM is based on the solution of selected beams of radiation and on the subsequent computation of the radiation sources, which combine the finite difference control volumes of the flow procedure due to the passage of the beams. The individual directions of rays are specified in advance rather than being chosen at random. The change in spectral intensity of the ray passing through the absorbing and emitting medium, I_ν, can be written as

$$\frac{dI_\nu}{d\kappa_\nu} = -I_\nu + I_{b\nu} \tag{4}$$

where κ_ν is the optical depth defined as $\kappa_\nu = \int_0^s k_\nu ds^*$ where $s^* = 0$ is at a cell entry and k_ν denotes the spectral absorption coefficient of the gas mixture. ν is spectrum wavenumber and $I_{b\nu}$ is the spectral blackbody intensity. The net gain of radiation energy $q_{r,n-1/2}$ through the computational cell $[r_{n-1}, r_n]$, whose gradient constituent a source term in the energy conservation equation, can be evaluated once the intensities along all the left and right traveling rays are known. For spherical geometry, the gradient of $q_{r,n-1/2}$ is obtained by integration of the net intensity over all solid angles in a discretised form and can be written as [47]

$$(\nabla \cdot q_r)_{n-1/2} = \left(\frac{1}{r^2}\frac{\partial(r^2 q_r)}{\partial r}\right) = \frac{8\pi\sum_{i=1}^{N}\sum_{j=1}^{M}(I_{n,ij}r_n^2 - I_{n-1,ij}r_{n-1}^2)\cos\theta_i \Delta\nu_j \Delta\Omega_i}{(r_n - r_{n-1})(r_n + r_{n-1})^2} \tag{5}$$

where $n = 2, \ldots, NG$ (NG is the number of grids), $I_{n,ij}$ is the radiation intensity of ray i at grid n. $\Delta\theta$ is given by $(\pi/2)/N$, θ_i by $\theta_i = (\pi/2)/N \cdot i$ and $\Delta\Omega_i = \sin\theta_i \Delta\theta_i$. M is the total number of bands and N is the number of rays. For the radiation property model of gas species, a modified wide band model was used, which assumes the absorption and emission of infrared radiation by a particular gas mainly occur in several relatively wideband. Thirteen bands were considered for CO_2, CO and H_2O altogether. They are the 2.0, 2.7, 4.3, 9.4, 10.4 and 15 μm vibrational–rotational bands of CO_2, the 4.7 and 2.35 μm vibrational–rotational bands of CO, and the 1.38, 1.87, 2.7 and 6.3 μm vibrational–rotational bands and a pure rotational band of H_2O.

4. Results and discussion

4.1. Laminar burning velocities

Experiments in microgravity are essential for measuring near-limit burning velocities. For slow-burning mixtures [14,15], flames in 1-g become observably buoyant, with the flame forming a mushroom shape and reaching the top of the chamber before the bottom. In microgravity, these flames remained spherical during propagation, making it possible to measure flame radius and thus to determine flame speed and stretch rate. For all flames considered here, the flame surface remained smooth at the early stage of the propagation process and no preferential-diffusion instability was observed. Ignition sparks might result in irregular ignition kernels, but irregular structures quickly smoothed out and the flame kernel quickly became spherical. For very slow flames, however, the effect of irregular ignition kernels was larger because it took a longer time for the slow-propagating surface to catch up with the rest of the surface.

Fig. 1 shows the measured and computed burning velocities as functions of the molar concentration of diluents for stoichiometric CH_4/air flames at normal temperature and pressure (NTP). The diluents considered are N_2, Ar, He, and CO_2. The laminar burning velocities presented here are unstretched values, $S_{L\infty}$, determined by applying Eq. (2) to the measured values of S_L and K, and are reported in Table 1. The estimated Lewis number (Le) is also reported in Table 1 for each reactant mixture. The computed unstretched burning velocities were obtained from both the steady-state planar flame simulations using PREMIX [16] and the spherically-expand-

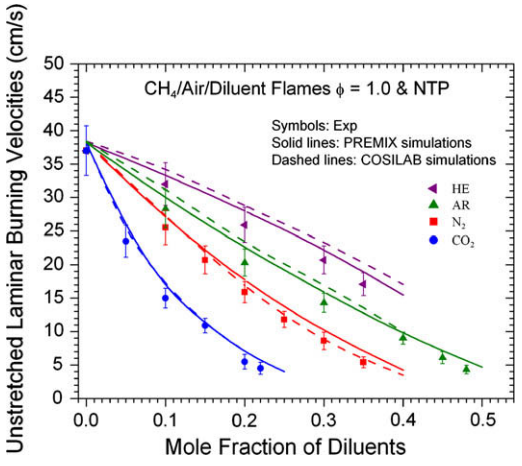

Fig. 1. Measured (symbols) and computed (lines) laminar burning velocities as functions of the mole fractions of helium, argon, nitrogen and carbon dioxide for adiabatic, premixed CH_4/air/diluent flames at $\phi = 1.0$ and NTP. Solid lines: simulation results for the planar premixed flames using PREMIX; dashed lines: simulation results for the spherically-expanding flames using COSILAB.

ing flame simulations using COSILAB [36]. The computed velocities shown in Fig. 1 are for adiabatic flames without consideration of radiation. Effects of radiation emission and absorption on flame properties, particularly for near-limit flames, will be discussed later in Section 3. For the COSILAB simulations, the methodology to obtain $S_{L\infty}$ was similar to the experiment: $S_{L\infty}$ was obtained by extrapolating the stretched velocities S_L as a function of the local stretch rate to zero stretch (Eq. (1)). In addition, the data for processing were limited to $r > 1.5$ cm to avoid ignition disturbances. The density ratios needed to determine S_L were the same as those for the experiments, which were computed assuming adiabatic constant-pressure combustion using the adiabatic equilibrium algorithms of McBride et al. [38].

The results in Fig. 1 show that all diluents considered here cause flame speed to decrease as their concentration is increased. Similar to the conclusions from previous studies [3,14,15], the capabilities of the diluents to reduce burning velocity at any fixed diluent concentration increases in the order He < Ar < N_2 < CO_2, with CO_2 being most effective. The computed $S_{L\infty}$ from PREMIX and COSILAB simulations generally agree well with each other. The flame speeds predicted using COSILAB are slightly higher than those using PREMIX for the helium and argon-diluted flames.

The lowest measured burning velocity $S_{L\infty}$ shown in Fig 1 is around 3–5 cm/s for the CO_2, N_2 or Ar diluted flames (except He). Note the mole fraction of the diluent that corresponds to the lowest burning velocity, however, is not the measured flammability limit, which is a topic that will be discussed in the next section. Helium is an exception: the lowest burning velocity we could measure for the helium-diluted flames is about 15 cm/s at a helium mole fraction of 38%, above which the ignition kernel dissipated and the flame did not propagate to the entire chamber, even though much higher ignition energy was used.

4.2. Markstein lengths and numbers

The measured and computed Markstein length (L) and Markstein number (Ma) are plotted as functions of the mole fractions of diluents for stoichiometric CH_4/air/diluent flames in Figs. 2 and 3, respectively. As shown in Table 1, the estimated Lewis number remains almost constant with N_2-dilution or Ar-dilution, and decreases only slightly with CO_2-dilution. It, however, increases with increasing mole fraction of helium.

The measured Markstein length and Markstein number have reasonable agreement with the computed values using COSILAB. For the Ar, N_2, and CO_2-diluted flames, the Markstein length varies little with increasing mole fraction of the diluents, except that a sudden increase was observed at 30–40% N_2-diltuion near extinction limit (Fig. 2). The nearly constant Markstein length can be explained by the fact that addition of Ar, N_2, and CO_2 does not significantly alter the preferential diffusion behavior of the mixture. The corresponding Markstein number of these mixtures, as shown in Fig. 3, decreases when the diluent mole fraction increases. This is because the flames become thicker and slower with higher diluent concentrations. The trend for the helium-diluted flames, however, is different. Both the Markstein length and Markstein number increase with increasing mole fraction of helium. The different trend observed in Figs. 2 and 3 is attributed to the much larger diffusivity of helium compared to O_2, N_2, Ar, or CO_2.

4.3. Extinction limits

Research on flammability limits is one of the fundamental areas of combustion science, and information on the flammability limits of mixtures of fuel and oxidant, with or without diluents, is important for the prevention and suppression of accidental fires. In this study, the maximum concentration of a diluent at the extinction limit is of interest because it is a measure of the efficiency of the diluents for preventing or suppressing a fire. The extinguishing diluent concentration was determined by systematically varying the composition and ignition energy and the limiting condition was found by successive experiment trials. A successful ignition means that a flame kernel initially produced by the ignition spark can propagate throughout the combustion chamber. Failure to ignite means the hot gas kernel from the ignition spark quickly dissipates and no flame propagation is observed. We also used a pressure transducer to record the pressure history within the chamber. A successful ignition was accompanied by a rapid increase of pressure inside the chamber, whereas failure to ignite was accompanied by no pressure increase after the ignition spark.

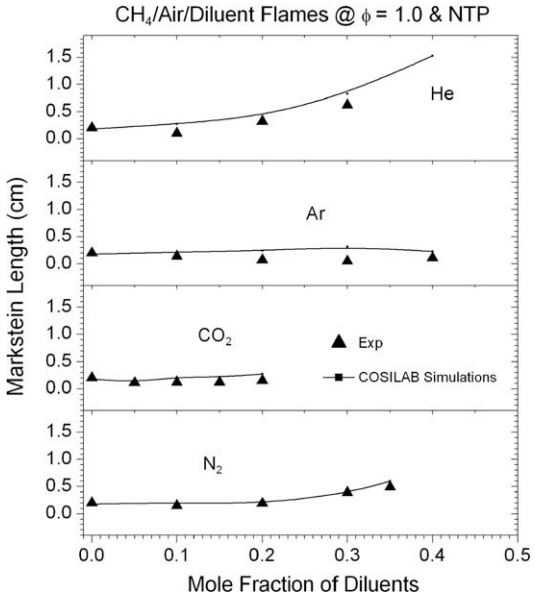

Fig. 2. Measured (symbols) and computed (lines) Markstein lengths as functions of the mole fractions of helium, argon, nitrogen and carbon dioxide for adiabatic, premixed CH_4/air/diluent flames at $\phi = 1.0$ and NTP.

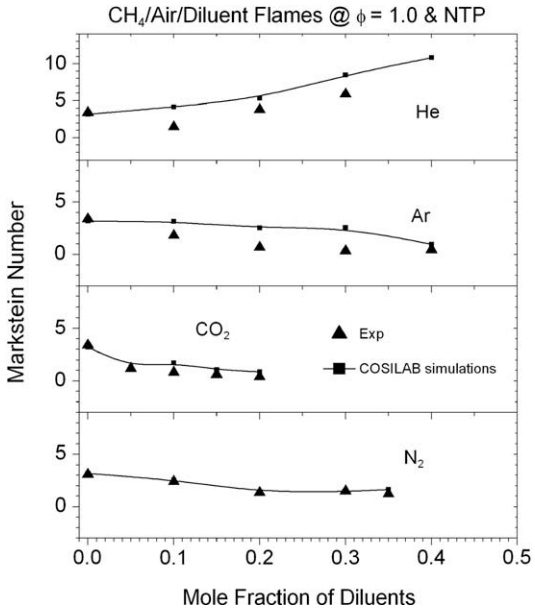

Fig. 3. Measured (symbols) and computed (lines) Markstein numbers as functions of the mole fractions of helium, argon, nitrogen and carbon dioxide for adiabatic, premixed CH_4/air/diluent flames at $\phi = 1.0$ and NTP.

Table 2
Extinguishing concentration of the diluents for CH_4/air flames at $\phi = 1.0$ and NTP.

Diluent	X_D[a] by this work	X_D by Coward and Jones [49]	X_D by Liao et al. [2]	X_D by Yamaoka and Tsuji [50]
He	38	39	–	–
Ar	51	48	54	–
N_2	39	37	40	38
CO_2	22	23	29	–

[a] X_D is the diluent concentration in the reactant mixture.

Table 2 shows the measured concentration of each diluent at extinction for stoichiometric CH_4/air flames at NTP, considering helium, argon, nitrogen, and carbon dioxide as diluents. X_D is the diluent molar concentration in the reactant mixtures. Also shown in Table 2 are the flammability limits measured by Coward and Jones using the explosion burette apparatus developed at US Bureau of Mines [49], by Liao et al. [2] using a tubular flame burner, and by Yamaoka and Tsuji [50] using twin flames, respectively. The present limits are close to those of Coward and Jones, but systematically lower than those of Liao et al. and Yamaoka and Tsuji for most cases. From a theoretical point of view, limits arise because mechanisms such as chain-termination reactions, heat losses due to conduction or radiation, and preferential-diffusion, eventually dominate the energy-releasing chemical reactions and cause extinction at the flammability limit. Flammability limits also depend on the apparatus. The broader flammability limits using the tubular burner method or the twin flame method, as shown in Table 2, may be because there is less heat loss in the burnt gas region than in the case of the spherical flames. In addition, spherically-expanding flames have larger stretch rates at the early propagation stage, which may also explain the lower limits. The slight difference between the present measurements and those by Coward and Jones may be due to gravity, as buoyant convection may affect extinction limits [51,52].

If the effectiveness of the diluents are evaluated based on their extinguishing concentrations, the ranking is $Ar < He \approx N_2 < CO_2$. CO_2 is the most effective with the lowest concentration mainly due to its large heat capacity. The limit behavior of helium is more complex. It is as effective as nitrogen but more effective than argon. As shown in Fig. 1, for a given diluent concentration, helium-diluted flames have higher burning velocities than argon flames due to higher mass and thermal diffusivity. The results in Table 2, however, show that helium is more effective than argon in terms of the extinguishing concentration. Note the limiting Ar, N_2 and CO_2 mixtures have a $Le \approx 1$, while the limiting helium mixture has a $Le \approx 4$, as shown in Table 1. When the helium concentration is above 38%, we observed that the ignition kernel stopped propagating very early, even though the ignition energy was significantly increased.

To evaluate the minimum ignition energy required to ignite a premixed mixture, the classical ignition analysis based on flame kernel propagation [53] was used here, which shows that the minimum ignition energy can be expressed as

$$E_{ign} = 61.6\left(\frac{c_P}{R_b}\right)\frac{(T_b - T_u)}{T_b}\left(\frac{\alpha}{S_L}\right)^3,$$

where c_P is the heat capacity, T_b and T_u is the temperature of burned and unburned gas, R_b is the critical radius, α is the thermal diffusivity, and S_L is the laminar burning velocity. The quantity R_b is defined such that a flame will not propagate if the actual radius is smaller than this critical value. E_{ign} to be supplied by the spark is the energy required to heat the critical gas volume from its initial state to the flame temperature, and $E_{ign} \sim \alpha^3$, assuming other parameters are constants. Therefore, because α_{He} is approximately nine times higher than α_{Ar}, the near-limit helium mixture would require about ~730 times higher ignition energy than the argon mixture if we assume that both flames have the same velocity. In addition, a recent theoretical study of Chen and Ju [54] shows that at intermediate Lewis numbers, E_{ign} increases exponentially with the increase of Le. Therefore, the present measured limit may be the ignition limit due to the extremely high ignition energy required.

Besides the minimum ignition energy, flame/stretch interaction may also contribute to the complex limit behavior of helium. The instantaneous effect of stretch on the flame is controlled by a generalized stretch factor [55]

$$\sigma = \frac{Ze}{2}\left(\frac{1}{Le} - 1\right)Ka,$$

where Ze, Le, and Ka are the Zel'dovich number, the Lewis number, and the Karlovitz number, respectively. The flame temperature and propagating speed are increased from the unstretched, adiabatic values for $\sigma > 0$, and decreased for $\sigma < 0$. Since the outwardly-propagating spherical flames have positive stretch rate, the above equation indicates that the flame temperature and flame speed are decreased for $Le > 1$ mixtures and increased for $Le < 1$ mixtures. Therefore, for the near-limit helium mixtures ($Le > 1$), stretch suppresses flame propagation. A competition between stretch and energy supplied by the ignition source can cause the extinction of the propagating flame if the ignition energy is not sufficient to drive the flame front to a radius at which stretch effects are reduced.

Overall, extinction of the flames by CO_2, N_2, and Ar is likely caused by the flame temperature dropping and radiative heat losses, and thus chemical reactions are not sustained. Flame extinction by helium, however, is mainly due to the high Lewis number effect. Due to the high diffusivity of helium, much higher minimum ignition energy is required. Furthermore, stretch suppresses flame propagation and can cause flame extinction.

4.4. Effects of radiative emission and absorption

It is well known that radiative heat loss becomes increasingly important near flammability limits. Radiation, combined with stretch, can change flame dynamics and extinguishing processes. Additionally, recent studies [34] have shown that the reabsorption effect of CO_2 can be significant in some situations and an optically-thin model may not be appropriate. Motivated by this, we used two radiation models in the present COSILAB simulations: an optically-thin limit model and an optically-thick model that solves the radiative transfer equation using DTM. For the radiation property of gas species, gray gas assumption was used for the optically-thin limit model and a modified wide band model was used for the optically-thick model. In the following, our discussion will focus on the CO_2-diluted flames as CO_2 is a strong emitter and absorber compared to the other diluents.

Fig. 4 compares the measured and computed burning velocities of the CH_4/air/CO_2 flames at various diluent concentrations. It can be seen that the optically-thin model underpredicts flame speed. The DTM method with a modified wide band model has better agreement with the measurements in the near-limit region. It, however, still overpredicts flame speed. The difference between the computed flame speeds using the two radiation models increases with increasing CO_2 concentration.

To understand the effects of radiative emission and absorption of CO_2 on the transient flame propagation process, we chose to discuss a near-limit CH_4/air flame with 20% CO_2 addition. Fig. 5 shows the measured and computed flame propagation speed relative to burned gases as a function of radius. The computed burned gas flame speeds were obtained with an optically-thin model (dashed line) and with the DTM model (solid line). It can be seen that radiation does not play an important role during the early stage of

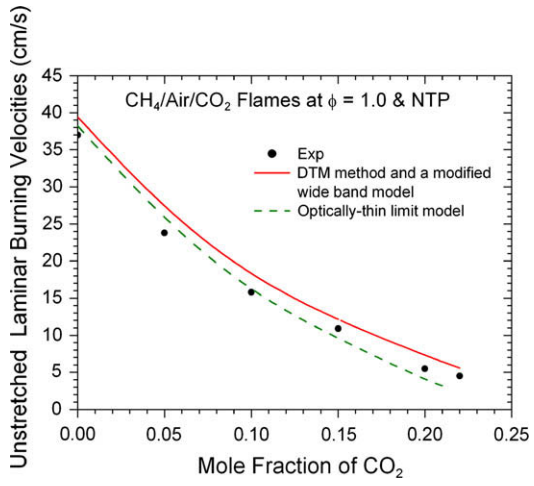

Fig. 4. Measured (symbols) and computed (lines) laminar burning velocities as a function of the mole fraction of carbon dioxide for premixed CH_4/air/CO_2 flames at $\phi = 1.0$ and NTP. Solid line: DTM method and a modified wide band model; dashed line: optically-thin limit model.

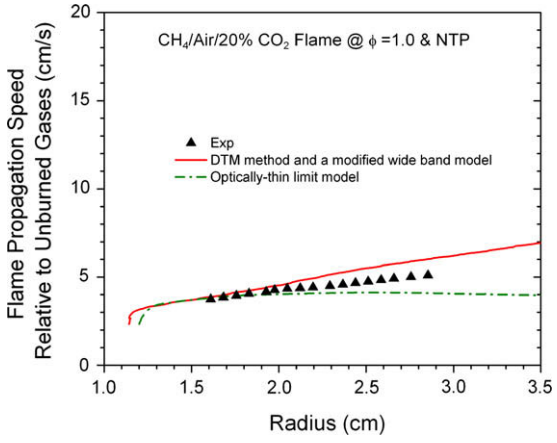

Fig. 5. The measured (symbols) and computed (lines) flame propagation speed relative to burned gases as a function of flame radius for the CH_4/air/20% CO_2 flame at $\phi = 1.0$ and NTP. Solid line: DTM method and a modified wide band model; dashed line: optically-thin limit model.

flame propagation when r is small, e.g., $r < 1.5$ cm. Radiation becomes increasingly important when r becomes large. After the initial flame propagation stage, the flame speed predicted by the optically-thin limit model decreases due to heat losses to the cold ambient gases. On the contrary, the flame speed predicted by the optically-thick model increases with radius. This is mainly because the unburned gases absorb heat from the hot zone, which results in elevated temperature of the unburned gases and thus increases flame propagation speed. The optically-thick model still overpredicts flame speed, indicating that a more sophisticated radiation property model such as a narrow band model may be needed.

The observed variation of flame speed due to radiative emission or absorption also raises a concern on the linear extrapolation method which has been widely used to extract unstretched burning velocities from spherically-expanding flames. Strictly speaking, the linear relation (Eq. (4)) between stretched flame speed and stretch rate is based on the assumption of small stretch and adiabatic flames. For radiating near-limit flames, however, flame speed variation due to radiation does not have a linear dependence on flame stretch. Therefore, for such flames, a non-linear extrapolation method that includes the effect of radiation may be more appropriate.

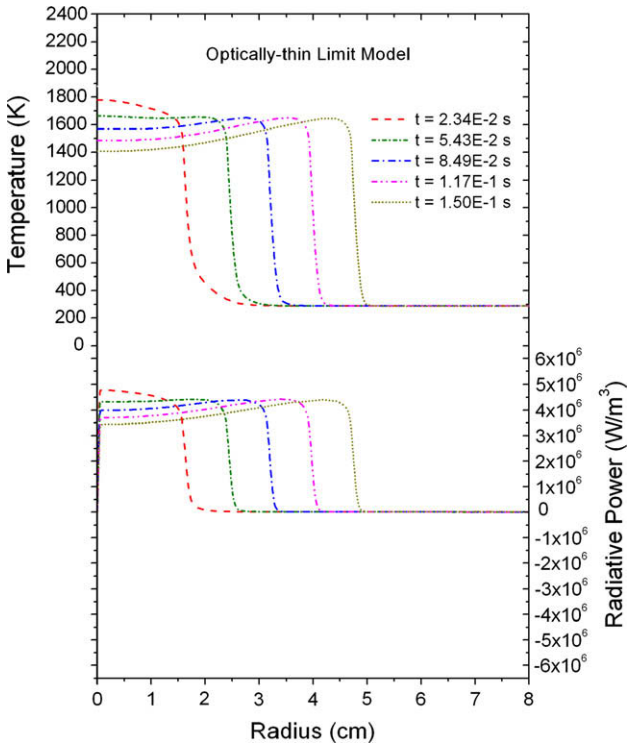

Fig. 6. The computed temperature (top) and radiative power (bottom) as a function of radius at various times for the spherically expanding CH_4/air/20% CO_2 flame at $\phi = 1.0$ and NTP using an optically-thin radiation model. Ignition occurs at $t = 0$.

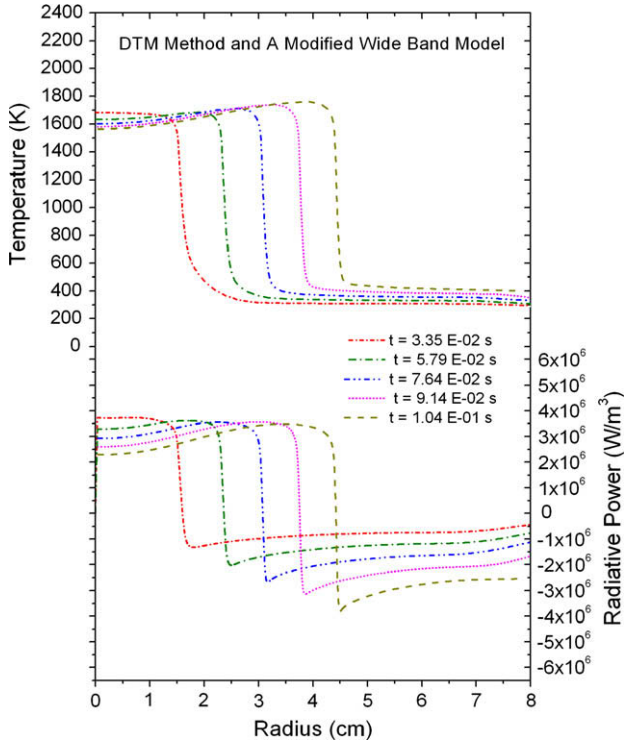

Fig. 7. The computed temperature (top) and radiative power (bottom) as a function of radius at various times for the spherically expanding CH_4/air/20% CO_2 flame at $\phi = 1.0$ and NTP using an optically-thick model based on the DTM method and a modified wide band model. Ignition occurs at $t = 0$.

Figs. 6 and 7 show the computed profiles of temperature and radiative power after ignition for the same near-limit flame as

discussed above (CH_4/air/20% CO_2) using the optically-thin radiation model (Fig. 6) and the DTM model (Fig. 7) respectively. As shown in Fig. 6, beyond the initial ignition stage, the temperature of burned gases continues to decrease as the flame propagates outwardly due to radiative heat loss to the cold ambient gases. The radiative power exhibits similar trend as the temperature. The peak temperature of the flame zone is around 1650 K, with only slight decrease (3–5 K) for each of the next time steps. Similar trends were observed in Fig. 7 using the DTM method and a modified wide band model: the temperature and radiative power of burned gases decrease as flame propagates outwardly. However, beyond the ignition stage the peak temperature of the reaction zone continues to increase as flame propagates outwardly. The radiative power profiles show that a significant amount of radiation heat loss from the hot products is reabsorbed by the cold ambient gases, resulting temperature increase of the unburned gases. The peak radiative power at the flame zone remains around 3.6×10^6 W/m^3 during flame propagation, with only slight decrease for each of the next time steps. The radiative power absorbed by the cold unburned gases, however, continues to increase with increasing r, due to the increasing volume of the hot burned gases. When the flame propagates to $r = 4.5$ cm, the peak radiation power absorbed by the cold gases is as large as the peak power emitted from the hot gases.

4.5. Chemical effect of CO_2 in flame suppression

The inert gases considered here belong to chemically passive or thermal-quenching types of flame suppressants, for which flame temperature, flame speed and reaction rate are reduced mainly due to dilution and thermal effects. This inhibition mechanism is different from chemically active types of suppressants such as Halons and Halon replacements. Active flame suppressants reduce reaction rate mainly by reducing the concentration of chain-carrying radicals (such as H and OH) in the reaction zone. For example, Halon 1301 (CF3Br) consumes H-atoms in the reaction zone through the reactions of $CF_3Br + H = CF_3 + HBr$, $H + HBr = H_2 + Br$ [56].

While N_2, Ar and He suppress a flame mainly by thermal effect, flame inhibition by CO_2 involves both physical and chemical effects, which have been studied by several researchers [57–60]. These studies show that CO_2 can be converted to CO through the reaction $CO + OH = CO_2 + H$, which is the dominant reaction pathway for the chemical participation of CO_2 in hydrocarbon flames. The competition of CO_2 for H radicals through this reaction with the most important chain-branching reaction $H + O_2 = O + OH$ can play a chemical inhibiting role that reduces the concentrations of important radicals, such as O, H, and OH, which subsequently reduces reaction rate and burning speed. Liu et al. [59] investigated the chemical effect of CO_2 on premixed CH_4 and H_2 flames numerically. Their results show that the chemical effect of CO_2 significantly reduces the burning velocity and the relative importance of the chemical effect of CO_2 increases with increasing CO_2 concentration.

To understand the importance of chemical effect of CO_2 in the overall flame suppression process, we did a numerical analysis to quantify the pure chemical effect of CO_2 in flame extinction. The approach is similar to the work of Liu et al. [59] and Park et al. [58,60]. This was done using the 1-D planar freely-propagating flame code PREMIX [16]. The thermodynamics and transport data were taken from CHEMKIN library [41,42]. The PRMEIX calculations used the same reaction mechanism, GRI-Mech 3.0 [43], as the transient COSILAB simulations. The strategy was to introduce an artificial species, named X, which has the same thermochemical, transport, and radiation properties as CO_2. However, this species does not participate in chemical reactions and is chemically inert.

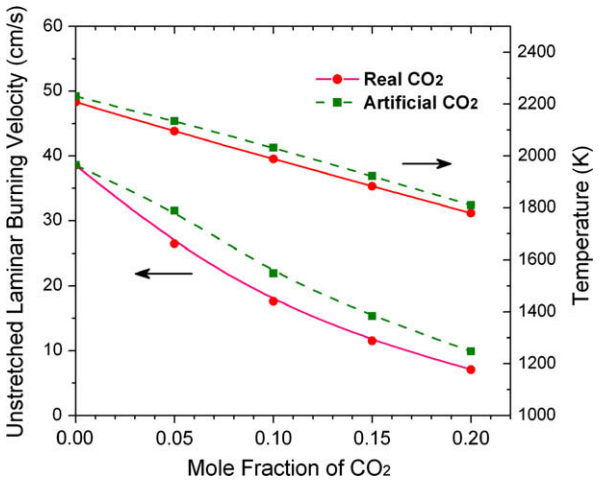

Fig. 8. The computed laminar burning velocity and burned gas temperature as a function of CO_2 mole faction for the adiabatic CH_4/air/CO_2 flames at $\phi = 1.0$ and NTP using PREMIX. Solid line: results for real CO_2; dashed line: results for artificial CO_2 which does not participate in chemical reactions.

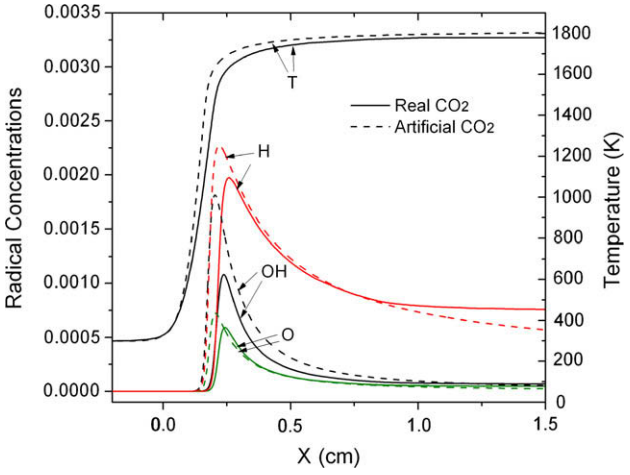

Fig. 9. The computed profiles of temperature and H, O, and OH radical concentrations for the adiabatic CH_4/air/20% CO_2 flame at $\phi = 1.0$ and NTP using PREMIX. Solid lines: results for real CO_2; dashed lines: results for artificial CO_2 which does not participate in chemical reactions.

Two solutions were obtained for each CO_2-diluted flame: one for real CO_2 which participates in chemical reactions, the other for the artificial species X excluding chemical effect. In addition, the species X has the same third-body collision efficiency as CO_2 in all relevant reactions.

Fig. 8 shows the computed laminar burning velocity and the temperature of burned gases of CO_2-diluted CH_4/air flames at NTP and $\phi = 1.0$ as a function of the mole fraction of CO_2 using the method described above. The solid line represents the results for real CO_2 and the dash line represents the results for artificial CO_2. In these calculations, radiation heat loss and reabsorption were not considered. As can be seen in Fig. 8, the chemical effect causes significant reduction in burning velocity and the degree of flame speed reduction increases with increasing CO_2 concentration. Near the limit condition, e.g., 20% CO_2 dilution by volume, the burning velocities are 7.1 cm/s and 9.9 cm/s for real CO_2 and artificial CO_2 respectively. This means chemical effect causes about 30% reduction in flame speed. The difference in flame temperature, however, is not significant, about 30–40 K for all CO_2 mole fractions.

Please cite this article in press as: L. Qiao et al., Combust. Flame (2010), doi:10.1016/j.combustflame.2010.04.004

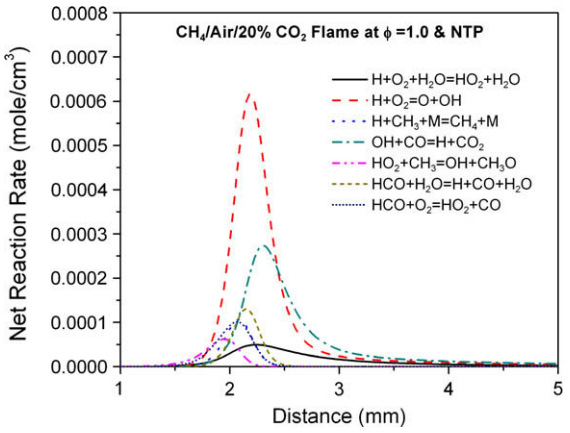

Fig. 10. Net reaction rates of stoichiometric CH_4/air/20% CO_2 flame at NTP.

We then plotted the computed temperature profile and the profiles of H, O, and OH radical concentrations for the near-limit CH_4/air/20% CO_2 flame (Fig. 9). The chemical effect of CO_2 reduces H, OH, and O radical concentrations. In particular, the maximum OH radical concentration for the artificial CO_2 case is almost twice as for the real CO_2 case. The radical reductions are mainly due to the reaction CO + OH = CO_2 + H, for which the reaction rate is the second largest among all elementary reactions and the first largest is the chain-branching reaction H + O_2 = O + OH, as shown in Fig. 10. The competition of CO_2 for H radical through CO + OH = CO_2 + H with H + O_2 = O + OH reduces H, OH, and O radical concentrations, leading to lower reaction rate and flame speed.

5. Conclusions

An experimental and numerical study was carried out to investigate the extinction behavior of premixed methane–air flames by various diluents including helium, argon, nitrogen and carbon dioxide in microgravity. The experiments were conducted using a short-drop free-fall facility that images flame propagation in a dropping chamber with stationary shadowgraph system. This enables accurate determination of the near-limit burning velocity. The maximum concentration of a specific diluent at the extinction limit was determined by systematically varying the composition and ignition energy and finding the limiting condition through successive experiment trials. The corresponding freely-propagating, planar flames were simulated using PREMIX. The spherically-expanding flames were simulated using the Spherical Flames Module of COSILAB considering detailed radiation models in spherical geometry. The following conclusions can be drawn based on the present experiments and computations:

1. Helium exhibits more complex limit behavior than the other diluents. Extinction of the flames by CO_2, N_2, and Ar is likely caused by the flame temperature dropping and radiative heat losses, and thus chemical reactions are not sustained. Flame extinction by helium, however, is mainly due to the high Lewis number effect. Due to the high thermal diffusivity, much higher ignition energy is required for helium mixtures than for the others. In addition, for spherically expanding helium-diluted flames, stretch suppresses flame propagation and can cause flame extinction.
2. Both an optically-thin model and an optically-thick model were employed in the spherically-expanding flame simulations using COSILAB to understand the effects of radiative emission and absorption on flame propagation and extinction. The results show that the optically-thin model underpredicts flame speed and the optically-thick model based on the DTM method and a modified wide band model has better agreement with measurements in the near-limit region. The simulation results show that a significant amount of radiation heat loss from the hot products is reabsorbed by the cold ambient gases, resulting in temperature increase in the unburned gas and the pre-heat zone. The peak radiative power due to absorption increases with time. The optically-thick model, however, still overpredicts flame speed, indicating that a more sophisticated radiation property model such as a narrow band model may be needed. In addition, a non-linear extrapolation method that includes the effect of radiation may be more appropriate for CO_2-diluted near-limit flames.
3. While N_2, Ar and He suppress a flame mainly by thermal effect, flame inhibition by CO_2 involves both physical and chemical effects. A numerical analysis shows that the pure chemical effect of CO_2 causes about 30% reduction in flame speed for the near-limit CH_4/air/20% CO_2 flame. The reduction is because CO_2 participates in the reaction CO_2 + H = CO + OH, which competes for H radicals with the most important chain-branching reaction H + O_2 = O + OH and thus reduces the concentrations of important radicals, such as O, H, and OH. This effect becomes more important when the CO_2 concentration becomes large.

Acknowledgments

The authors want to thank Dr. Hans Ernst of Rotexo GmbH & Co. KG for assistance in using COSILAB and for insightful discussions on the radiation models.

References

[1] D.M. Tucker, D.D. Drysdale, D.J. Rasbash, Combust. Flame 41 (3) (1981) 293–300.
[2] C. Liao, N. Saito, Y. Saso, Y. Ogawa, Fire Safety J. 27 (1) (1996) 49–68.
[3] N. Saito, Y. Ogawa, Y. Saso, C.H. Liao, R. Sakei, Fire Safety J. 27 (3) (1996) 185–200.
[4] M.S. Wu, J.B. Liu, P.D. Ronney, Proc. Combust. Inst. 27 (1998) 2543–2550.
[5] J.A. Senecal, Fire Safety J. 40 (6) (2005) 579–591.
[6] F. Takahashi, G.T. Linteris, V.R. Katta, Proc. Combust. Inst. 31 (2007) 2721–2729.
[7] M.K. Chernovsky, A. Atreya, H.G. Im, Proc. Combust. Inst. 31 (1) (2007) 1005–1013.
[8] S. Tang, H.G. Im, A. Atreya, Combust. Flame 157 (1) (2010) 127–136.
[9] C.K. Law, G.M. Faeth, Prog. Energy Combust. Sci. 20 (1) (1994) 65–113.
[10] M. Kono, K. Ito, T. Niioka, T. Kadota, J. Sato, Proc. Combust. Inst. 26 (1996) 1189–1199.
[11] R.K. Cheng, B. Bedat, Combust. Flame 116 (3) (1999) 360–375.
[12] H. Zhang, F.N. Egolfopoulos, Proc. Combust. Inst. 28 (2000) 1875–1882.
[13] P.D. Ronney, in: H. Ross (Ed.), Microgravity Combustion: Fires in Free Fall, Academic Press, London, UK, 2001, pp. 35–82.
[14] L. Qiao, Y.X. Gu, W.J.A. Dam, E.S. Oran, G.M. Faeth, Proc. Combust. Inst. 31 (2007) 2701–2709.
[15] L. Qiao, Y. Gu, W.J.A. Dam, E.S. Oran, G.M. Faeth, Combust. Flame 151 (2007) 196–208.
[16] R.J. Kee, J.F. Grcar, M.D. Smooke, J.A. Miller, A FORTRAN Program for Modeling Steady Laminar One-dimensional Premixed Flames, Rept. SAND85-8240, Sandia National Labs., Albuquerque, NM, 1993.
[17] J.R. Farmer, P.D. Ronney, Combust. Sci. Technol. 73 (4–6) (1990) 555–574.
[18] J.D. Buckmaster, G. Joulin, P.D. Ronney, Combust. Flame 84 (3–4) (1991) 411–422.
[19] G. DixonLewis, Proc. Roy. Soc. Lond. Ser. A – Math. Phys. Eng. Sci. 452 (1996) 1857–1884.
[20] K. Maruta, M. Yoshida, Y.G. Ju, T. Niioka, Proc. Combust. Inst. 26 (1996) 1283–1289.
[21] R. Blouquin, P. Cambray, G. Joulin, Combust. Sci. Technol. 128 (1–6) (1997) 231–255.
[22] J. Buckmaster, Combust. Theory Model. 1 (1) (1997) 1–11.
[23] Y.G. Ju, H.S. Guo, K. Maruta, F.S. Liu, J. Fluid Mech. 342 (1997) 315–334.
[24] Y.G. Ju, H.S. Guo, K. Maruta, T. Niioka, Combust. Flame 113 (4) (1998) 603–614.
[25] Y.G. Ju, G. Masuya, F.S. Liu, H.S. Guo, K. Maruta, T. Niioka, Proc. Combust. Inst. 27 (1998) 2551–2557.
[26] Y.G. Ju, H.S. Guo, F.S. Liu, K. Maruta, J. Fluid Mech. 379 (1999) 165–190.
[27] Y.G. Ju, H. Matsumi, K. Takita, G. Masuya, Combust. Flame 116 (4) (1999) 580–592.

[28] H.S. Guo, Y.G. Ju, T. Niioka, Combust. Theory Model. 4 (4) (2000) 459–475.
[29] Y. Ju, G. Masuya, F. Liu, Y. Hattori, D. Riechelmann, Int. J. Heat Mass Transfer 43 (2) (2000) 231–239.
[30] F. Liu, G.J. Smallwood, O.L. Gulder, Y. Ju, Combust. Flame 121 (1–2) (2000) 275–287.
[31] J.F. Wang, T. Niioka, Proc. Combust. Inst. 29 (2002) 2211–2217.
[32] J.K. Bechtold, C. Cui, M. Matalon, Proc. Combust. Inst. 30 (2005) 177–184.
[33] G. Dixon-Lewis, Proc. Roy. Soc. A – Math. Phys. Eng. Sci. 462 (2006) 349–370.
[34] Z. Chen, M. Qin, B. Xu, Y.G. Ju, F.S. Liu, Proc. Combust. Inst. 31 (2007) 2693–2700.
[35] Z. Chen, Y.G. Ju, Int. J. Heat Mass Transfer 51 (25–26) (2008) 6118–6125.
[36] COSILAB, Combustion Simulation Laboratory, SOFTPREDICT.
[37] R.A. Strehlow, L.D. Savage, Combust. Flame 31 (2) (1978) 209–211.
[38] B.J. McBride, M.A. Reno, S. Gordon, CET93 and CETPC: An Interim Updated Version of the NASA Lewis Computer Program for Calculating Complex Chemical Equilibrium with Applications, NASA TM 4557, 1994.
[39] G.H. Markstein, Non-steady Flame Propagation, Pergamon, New York, 1964.
[40] P. Clavin, Prog. Energy Combust. Sci. 11 (1) (1985) 1–59.
[41] R.J. Kee, G. Dixon-Lewis, J. Warnatz, M.E. Coltrin, J.A. Miller, A FORTRAN Computer Code Package for the Evaluation of Gas-phase, Multicomponent Transport Properties, Rept. SAND86-8246, Sandia National Labs., Albuquerque, NM, 1992.
[42] R.J. Kee, F.M. Rupley, J.A. Miller, The CHEMKIN Thermodynamic Data Base, Rept. SAND87-8215B, Sandia National Labs., Albuquerque, NM, 1992.
[43] D.M.G. Gregory, P. Smith, Michael Frenklach, Nigel W. Moriarty, Boris Eiteneer, Mikhail Goldenberg, C. Thomas Bowman, Ronald K. Hanson, Soonho Song, William C. Gardiner, Jr., Vitali V. Lissianski, and Zhiwei Qin. <http://www.me.berkeley.edu/gri_mech/>.
[44] B. Rogg, RUN-1DL: The Cambridge Universal Laminar Flame Code. second ed. Technical Report CUED/A-THERMO/TR39, Department of Engineering, University of Cambridge, 1991.
[45] R.J. Kee, F.M. Rupley, J.A. Miller, CHEMKIN II: A Fortran Chemical Kinetics Package for the Analysis of Gas Phase Chemical Kinetics, Rept. SAND89-8009B, Sandia National Labs., Albuquerque, NM, 1993.
[46] SigmaPlot® 2004, Systat Software, Inc.
[47] Y. Liu, PhD thesis, Department of Engineering, University of Cambridge, 1994.
[48] J.Y. Chen, Y. Liu, B. Rogg, Lecture Notes in Physics Monographs, vol. 15, Springer, Berlin/Heidelberg, 1993. pp. 196–223.
[49] H. Coward, C. Jones, Limits of Flammability of Gases and Vapors, US Government Printing Office, Washington, DC, 1952.
[50] I. Yamaoka, H. Tsuji, Combust. Flame 86 (1–2) (1991) 135–146.
[51] J. Jarosinsky, R.A. Strehlow, A. Azarbarzin, Proc. Combust. Inst. 19 (1982) 1549–1557.
[52] J.D. Buckmaster, D. Mikolaitis, Combust. Flame 45 (1982) 109–119.
[53] S.R. Turns, An Introduction to Combustion, second ed., McGraw Hill, 2000.
[54] Z. Chen, Y. Ju, Combust. Theory Model. 11 (3) (2007) 427–453.
[55] C.K. Law, Combustion Physics, Cambridge University Press, New York, 2006.
[56] C.H. Kim, O.C. Kwon, G.M. Faeth, J. Propul. Power 18 (5) (2002) 1059–1067.
[57] F.S. Liu, H.S. Guo, G.J. Smallwood, O.L. Gulder, Combust. Flame 125 (1–2) (2001) 778–787.
[58] J. Park, K. Lee, E. Lee, Int. J. Energy Res. 25 (6) (2001) 469–485.
[59] F.S. Liu, H.S. Guo, G.J. Smallwood, Combust. Flame 133 (4) (2003) 495–497.
[60] J. Park, D.J. Hwang, J.G. Choi, K.M. Lee, S.I. Keel, S.H. Shim, Int. J. Energy Res. 27 (13) (2003) 1205–1220.

Please cite this article in press as: L. Qiao et al., Combust. Flame (2010), doi:10.1016/j.combustflame.2010.04.004